Nonlinear Laser Dynamics with Suppressed Time-delay Signatures by FBGs

Song-Sui Li[1], Xiao-Zhou Li[1], Jun-Ping Zhuang[1], and Sze-Chun Chan[1,2,*]

[1]Department of Electronic Engineering, City University of Hong Kong, Hong Kong, China
[2]State Key Laboratory of Millimeter Waves, City University of Hong Kong, Hong Kong, China
*Email: scchan@cityu.edu.hk

Abstract– Chaotic dynamics in a single-mode semiconductor laser subject to optical feedback from fiber Bragg gratings (FBGs) is investigated. Obtained from the inverse Fourier transform on the magnitude of the optical spectra, the coherence function evaluates the suppression of the time-delay information. The intensity autocorrelation function time-delay signature (ACF-TDS) and coherence function time-delay signature (CF-TDS) are found to be sensitive to the FBG bandwidth. The FBG feedback with proper bandwidth and positive detuning frequency can achieve both ACF-TDS concealment and CF-TDS minimization in chaotic oscillation. Moreover, the TDS-optimized chaos can be generally obtained over a range of feedback delay times. Besides, comparing to conventional mirror feedback, the FBG feedback suppresses the ACF-TDS by more than an order of magnitude in the experiments.

1. Introduction

Nonlinear dynamics of semiconductor lasers have received attentions in recent applications [1-5, 18]. Chaotic dynamics is widely investigated because it is noise-like, broadband, and synchronizable. It has been utilized in novel applications such as chaos-based secure communication [3], high-speed random bit generation [2, 18], and chaotic ranging [5]. Generally, inducing optical feedback into a semiconductor laser is the simplest way to obtain chaotic dynamics as only one laser is involved [6]. However, the feedback time-delay information can be extracted through the chaotic output analysis. Identification of the time-delay signature (TDS) in the autocorrelation of chaotic intensity time series is the most popular method for the delay time detection [7-12, 15, 16]. The TDS threatens the security in secure communication, limits the sampling rate in random bit generation, and introduces ambiguity in target detection.

Various approaches have been reported to solve this undesirable TDS problem. Rontani *et al*. has numerically demonstrated a pioneering work on TDS suppression in a single-mirror feedback scheme through optimizing the feedback strength at a relatively short feedback delay time, which is comparable to the period of the relaxation oscillation [7]. Other approaches that have been proposed include dual-path mirror feedback [8], polarization-preserved or polarization-rotated feedback [9, 15], and mutually coupled feedback using two lasers [10, 16]. These approaches perform TDS suppression, while compromise the hardware complexity by adopting multiple reflectors or multiple lasers. Recently, fiber Bragg gratings (FBGs) have been used in chaos generation as a simple method of TDS suppression [11, 12, 19]. Instead of a single mirror, an FBG is employed as a distributed reflector, which obscures the round-trip feedback delay times, hence leads to the TDS suppression. Comparing to the other approaches, the use of FBG feedback conceals TDS with relatively simple hardwares as it only involves coupling light into an FBG.

In this paper, a chaotic semiconductor laser subject to optical feedback from an FBG is investigated. In the simulation, besides the conventional intensity autocorrelation function (ACF), the so-called coherence function (CF), which equals to the inverse Fourier transform of the magnitude of the optical spectrum, is used for the TDS analysis as well. The evolution of the CF-TDS reveals the influences of the FBG bandwidth and detuning frequency from the laser on the identification of time-delay information. Feedback from the FBG with proper bandwidth and positive detuning frequency can achieve both ACF-TDS concealment and CF-TDS minimization in chaotic oscillation. Moreover, the TDS-optimized chaos can be generally obtained over a range of feedback delay times. In the experiment, chaos with ACF-TDS concealment has been obtained by using FBG feedback with a fixed delay time. Comparing to conventional mirror feedback, the FBG feedback suppresses the ACF-TDS by more than an order of magnitude.

2. Model

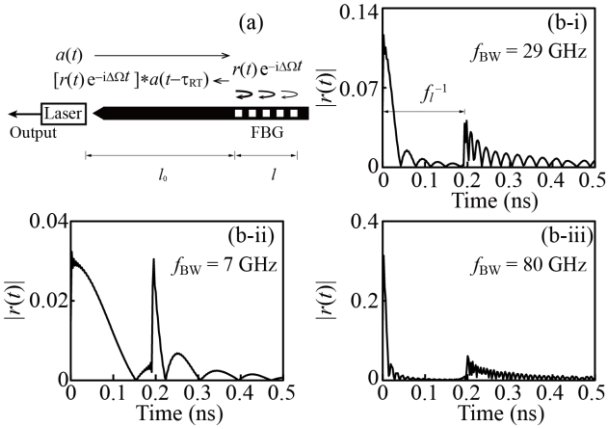

Fig. 1. (a) The schematic of a semiconductor laser subject to feedback from an FBG and (b) magnitude of the FBG impulse response $|r(t)|$, where (b-i), (b-ii), and (b-iii) correspond to f_{BW} = 29 GHz, 7 GHz, and 80 GHz, respectively, with f_l = 5 GHz.

Figure 1(a) shows the schematic of a single-mode semiconductor laser subject to distributed feedback from an FBG. The linearly polarized laser emission is directly coupled into a single-mode fiber appended with the FBG. It then experiences a distributed reflection and injects back into the laser. The FBG is uniform and has no birefringence. The central frequency of its reflection spectrum, namely the Bragg frequency, is detuned by Δf from the free-running frequency of the laser. The optical path length from the laser to the front-end of the FBG is denoted by l_0. The corresponding feedback round-trip delay time is $\tau_{\mathrm{RT}} = 2l_0/c$ with c being the speed of light in vacuum. This system can be described by the following rate equations [12]:

$$\frac{da}{dt} = \frac{1-\mathrm{i}b}{2}\left[\frac{\gamma_\mathrm{c}\gamma_\mathrm{n}}{\gamma_\mathrm{s}\tilde{J}}\tilde{n} - \gamma_\mathrm{p}(|a|^2-1)\right]a + \gamma_\mathrm{c}\xi_\mathrm{f}e^{\mathrm{i}\theta}[r(t)e^{-\mathrm{i}\Delta\Omega t}] * a(t-\tau_{\mathrm{RT}}) \quad (1)$$

$$\frac{d\tilde{n}}{dt} = -(\gamma_\mathrm{s}+\gamma_\mathrm{n}|a|^2)\tilde{n} - \gamma_\mathrm{s}\tilde{J}\left(1-\frac{\gamma_\mathrm{p}}{\gamma_\mathrm{c}}|a|^2\right)(|a|^2-1) \quad (2)$$

where the cavity decay rate $\gamma_\mathrm{c} = 5.36\times10^{11}\ \mathrm{s}^{-1}$, the spontaneous carrier relaxation rate $\gamma_\mathrm{s} = 5.96\times10^{9}\ \mathrm{s}^{-1}$, the differential carrier relaxation rate $\gamma_\mathrm{n} = 7.53\times10^{9}\ \mathrm{s}^{-1}$, the nonlinear carrier relaxation rate $\gamma_\mathrm{p} = 1.91\times10^{10}\ \mathrm{s}^{-1}$, the normalized bias current above threshold $\tilde{J} = 1.222$, the linewidth enhancement factor $b = 3.2$, the feedback phase $\theta = 0$, and the normalized feedback strength ξ_f is proportional to the coupling efficiency between the laser. The laser parameters correspond to a relaxation resonance frequency of $f_\mathrm{r} = 10.25$ GHz. They were extracted from a commercial communication laser [17]. The FBG feedback term, which is proportional to the delayed optical field amplitude $a(t-\tau_{\mathrm{RT}})$ convoluted with $r(t)e^{-i\Delta\Omega t}$, is the last term in Eq. (1), where $\Delta\Omega = 2\pi\Delta f$ is the angular frequency detuning of the Bragg frequency of the FBG away from the free-running frequency of the laser and $r(t)$ is the impulse response of the FBG at the rotating frame of the Bragg resonance frequency. Thus, $r(t)$ equals to the inverse Fourier transform of the reflection frequency response [13, 14]:

$$r(\Omega) = \Omega_{\mathrm{BW}}\times\left(2\Omega + \mathrm{i}\sqrt{{\Omega_{\mathrm{BW}}}^2-4\Omega^2}\coth\frac{\pi\sqrt{{\Omega_{\mathrm{BW}}}^2-4\Omega^2}}{2\Omega_l}\right)^{-1} \quad (3)$$

with FBG parameters $\Omega_{\mathrm{BW}} = 2\pi f_{\mathrm{BW}}$ and $\Omega_l = 2\pi f_l$. From $r(\Omega)$ in Eq. (3), the full width at half-maximum (FWHM) reflection bandwidth of the main lobe is approximately f_{BW} for a highly reflective FBG, whereas the reciprocal of the round-trip propagation time inside the FBG is f_l = 5.2 GHz, which is chosen throughout the simulation because it corresponds to a practical grating length of l = 20 mm with a refractive index of 1.444. The peak reflectivity of $\tanh^2(\pi\Omega_{\mathrm{BW}}/2\Omega_l)$ is attained at the Bragg frequency at $\Omega = 0$. Numerical simulations are conducted based on second-order Runge-Kutta integration of Eqs. (1)-(3) with time step 2.38 ps over a time span of 1.25 μs. The grating is chosen with $\theta = 0$. The feedback strength is $\xi_\mathrm{f} = 0.078$ throughout the simulation.

3. Numerical Results

Figures 1(b-i)-(b-iii) show the magnitude of the FBG impulse response $|r(t)|$ with f_{BW} = 29 GHz, 7 GHz, and 80 GHz, respectively. In Fig. 1(b-i), the FBG impulse response is confirmed as causal. It consists of two distinct components: a main reflection peak at time zero and a small peak at ${f_l}^{-1}$. As a result, the FBG can provide a distributed reflection. The peaks are separated by ${f_l}^{-1}$ = 0.19 ns, which is the round-trip propagation time inside the FBG [14]. Besides, comparing Figs. 1(b-i)-(b-iii), the width of the main reflection peak is inversely proportional to the FBG bandwidth f_{BW}. Roughly δ-function response can be achieved when the FBG is sufficiently broadband, as Fig. 1 (b-iii) shows.

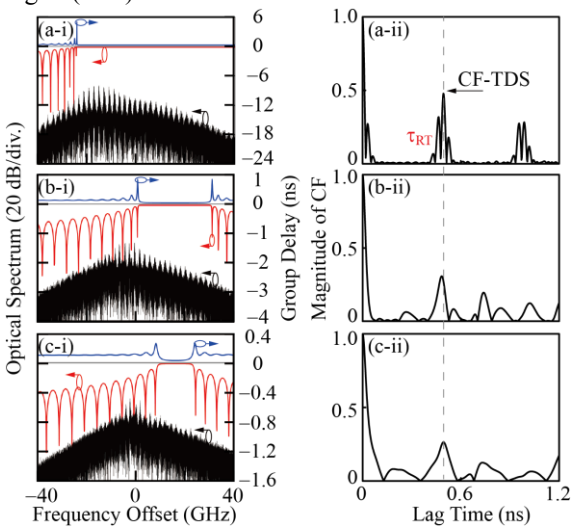

Fig. 2. Numerically calculated (i) optical spectrum and (ii) magnitude of CF. The frequency axis is offset to the free-running frequency of the laser. The chaotic optical spectra are shown in black. For reference, the optical reflectivity spectra of the FBG are shown in red, whereas the corresponding group delays are shown in blue. The FBG bandwidth f_{BW} = (a) 80 GHz, (b) 29 GHz, and (c) 13 GHz, respectively. The detuning frequency Δf = 16 GHz. The feedback round-trip delay time τ_{RT} = 0.47 ns.

Numerically calculated optical spectra of chaotic emissions are shown in black in Fig. 2(i), where the frequency axis is offset to the free-running frequency of the laser. For reference, the optical reflectivity spectra of the FBG are shown in red, while the corresponding group delays are shown in blue. The magnitude of the CF is shown in Fig. 2(ii). The FBG bandwidth f_{BW} = 80 GHz, 29 GHz, and 13 GHz in Figs. 2(a)-(c), respectively. The detuning frequency is Δf = 16 GHz. The feedback round-trip delay time is τ_{RT} = 0.47 ns.

In Fig. 2(a) with FBG bandwidth f_{BW} = 80 GHz, the bandwidth of the FBG is relatively broad comparing with the laser relaxation resonance frequency f_r. The main lobe

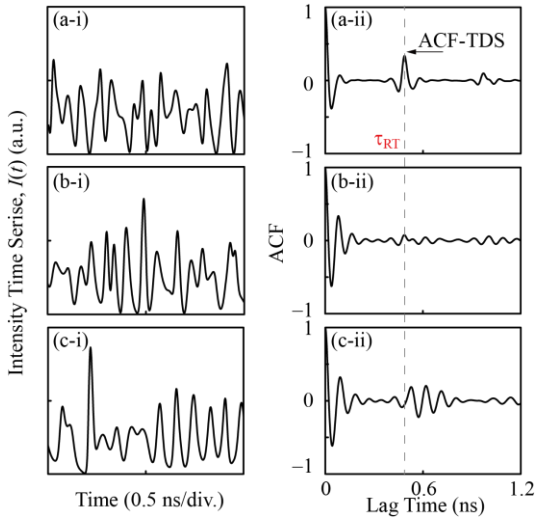

Fig. 3. Numerically calculated (i) intensity time series and (ii) the corresponding ACF. The FBG bandwidth f_{BW} = (a) 80 GHz, (b) 29 GHz, and (c) 13 GHz. The detuning frequency $\Delta f = 16$ GHz and the feedback round-trip delay time $\tau_{RT} = 0.47$ ns.

of the FBG covers most of the chaotic optical spectrum and does not induce much dispersion of the group delay, as shown in Fig. 2(a-i). Due to the antiguidance effect, a significantly red-shifted optical spectrum that spans a frequency range of over 10 GHz is observed. The enhanced peaks are at negative offset frequencies. However, in the spectrum, there are periodic peaks separated by about 2 GHz, which roughly corresponds to ${\tau_{RT}}^{-1}$. These peaks can be regarded as the external cavity mode structures. Such spectral features result in peaks at around τ_{RT} and its integer in the CF, which reveal the time-delay information in Fig. 2(a-ii). A clear CF-TDS unveils the delay time τ_{RT} as marked by the dashed line.

In Fig. 2(b), the FBG bandwidth f_{BW} = 29 GHz. The strongest emission peaks are now mainly found in the low frequency side lobes, as shown in Fig. 2(b-i). The frequency-dependent group delay experienced varies significantly, leading to an increase of chromatic dispersion. As a result, the FBG feedback obscures the information on the round-trip time delay. The periodicity, of the external cavity mode structures in Fig. 2(b-i) is less recognizable comparing with those in Fig. 2(a-i). This is further confirmed in Fig. 2(b-ii) that the CF-TDS is broadened and suppressed. Moreover, additional coherence peaks appear at different lag times, which induce uncertainty in the identification of CF-TDS.

In Fig. 2(c), with f_{BW} = 13 GHz, the strongest emission peaks move further away into the low frequency side lobes with the periodicity of the external cavity mode structures being even less recognizable in Fig. 2(c-i). The CF-TDS remains irregular as shown in Fig. 2(c-ii).

Figures 3(a)-(c) show the numerically calculated intensity time series and the ACFs which correspond to the optical spectra in Figs. 2(a)-(c). Column (i) of Fig. 3 shows the intensity time series $I(t) = |a(t)|^2$, while column (ii) shows the autocorrelation of $I(t)$ as a function of the lag time. In Fig. 3(a-i), the intensity time series is

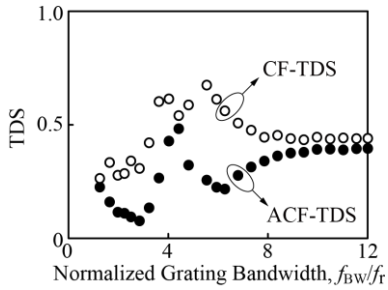

Fig. 4. ACF-TDS and CF-TDS as functions of the normalized grating bandwidth f_{BW}/f_r in closed and open symbols, respectively. The detuning frequency $\Delta f = 16$ GHz and the feedback round-trip delay time $\tau_{RT} = 0.47$ ns.

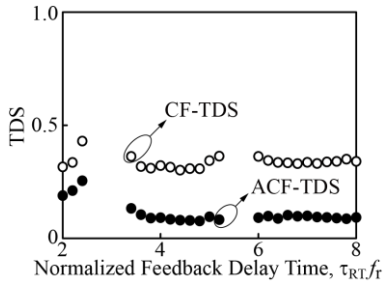

Fig. 5. ACF-TDS and CF-TDS as functions of the normalized feedback delay time $\tau_{RT}f_r$ in closed and open symbols, respectively. The FBG bandwidth f_{BW} = 29 GHz and the detuning frequency $\Delta f = 16$ GHz.

noise-like. It is hard to identify the time-delay information. However, when transformed into the ACF in Fig. 3(a-ii), the delay time τ_{RT} can be easily observed through the location of the ACF-TDS as marked by dashed line. In Fig. 3(b), the FBG bandwidth is f_{BW} = 29 GHz. the intensity time series is also noise-like as shown in Fig. 3(b-i). The ACF-TDS is significantly suppressed in Fig. 3(b-ii). Further reduces f_{BW} to 13 GHz, in Fig. 3(c-ii), the ACF-TDS becomes pronounced again, but the ACF-TDS peaks deviates away from τ_{RT}, which means a reduced accuracy in time-delay information detection.

Detailed investigation of ACF-TDS and CF-TDS as functions of the normalized grating bandwidth f_{BW}/f_r are shown in Fig. 4, where only chaotic oscillations are taken into account. The detuning frequency is kept at $\Delta f = 16$ GHz. The feedback round-trip delay time is kept at $\tau_{RT} = 0.47$ ns. Closed and open symbols correspond to ACF-TDS and CF-TDS, respectively. When the normalized grating bandwidth is relatively large, both the ACF-TDS and CF-TDS are nearly independent of f_{BW}/f_r. Because the FBG bandwidth f_{BW} is sufficiently broad, further increasing it will not change neither the reflection power nor the group delay in the optical frequency range of chaos. When f_{BW}/f_r is around 2.8, both ACF-TDS and CF-TDS are nearly minimized. Figure 4 shows that it is feasible to choose an FBG with proper f_{BW} so that both ACF-TDS and CF-TDS can get effective suppression at the same time under a positive detuning frequency.

Figure 5 shows the TDS as a function of the normalized feedback delay time $\tau_{RT}f_r$, where only chaotic oscillations are taken into account. The FBG bandwidth f_{BW} = 29 GHz and the detuning frequency $\Delta f = 16$ GHz are kept

constant. Closed and open symbols correspond to ACF-TDS and CF-TDS, respectively. In the normalized feedback delay time ranging from 4 to 8, both ACF-TDS and CF-TDS nearly remain unchanged. It is worth to mention that the TDS-optimized chaotic dynamics can be generally obtained over a range of feedback delay times. This significantly simplifies the operation in experiment.

Furthermore, experimental verifications are conducted to confirm TDS suppression using FBG feedback. Compared to using a conventional mirror, the FBG feedback suppresses ACF-TDS, by over 10 times, to less than 0.04 according to experimental measurements.

4. Conclusion

In summary, a single-mode semiconductor laser subject to optical feedback from an FBG is investigated. The ACF-TDS and CF-TDS are found to be sensitive to the FBG bandwidth. The FBG feedback with proper bandwidth and positive detuning frequency can suppress ACF-TDS and minimize CF-TDS in chaotic oscillations. Furthermore, the TDS-optimized chaos can be generally obtained over a range of feedback delay times. In the experiment, the FBG feedback suppresses the ACF-TDS to less than 0.04, which is about 10 times lower than that in conventional mirror feedback.

Acknowledgments

This work was supported by a grant from the Research Grant Council of Hong Kong, China (Project No. CityU 111213) and a grant from the National Natural Science Foundation of China (Grant 61308002).

References

[1] M. Sciamanna and K. A. Shore, "Physics and applications of laser diode chaos," *Nat. Photon.*, vol. 9, pp. 151–162, 2015.

[2] A. Uchida, K. Amano, M. Inoue, K. Hirano, S. Naito, H. Someya, I. Oowada, T. Kurashige, M. Shiki, S. Yoshimori, K. Yoshimura, and P. Davis, "Fast physical random bit generation with chaotic semiconductor lasers," *Nat. Photon.*, vol. 2, pp. 728–732, 2008.

[3] A. Argyris, D. Syvridis, L. Larger, V. Annovazzi-Lodi, P. Colet, I. Fischer, J. Garcia-Ojalvo, C. R. Mirasso, L. Pesquera, and K. A. Shore, "Chaos-based communications at high bit rates using commercial fibre-optic links," *Nature*, vol. 438, pp. 343–346, 2005.

[4] M. C. Soriano, J. Garcia-Ojalvo, C. R. Mirasso, and I. Fischer, "Complex photonics: Dynamics and applications of delay-coupled semiconductors lasers," *Rev. Mod. Phys.*, vol. 85, pp. 421–470, 2013.

[5] F. Y. Lin and J. M. Liu, "Diverse waveform generation using semiconductor laser for radar and microwave applications," *IEEE J. Quantum Electron.*, vol. 40, pp. 682–689, 2004.

[6] V. Annovazzi-Lodi, A. Scire, M. Sorel, and S. Donati, "Dynamic behavior and locking of a semiconductor laser subjected to external injection," *IEEE J. Quantum Electron.*, vol. 34, pp. 2350–2357, 1998.

[7] D. Rontani, A. Locquet, M. Sciamanna, and D. S. Citrin, "Loss of time-delay signature in the chaotic output of a semiconductor laser with optical feedback," *Opt. Lett.*, vol. 32, pp. 2960–2962, 2007.

[8] J. G.Wu, G. Q. Xia, and Z.M.Wu, "Suppression of time delay signatures of chaotic output in a semiconductor laser with double optical feedback," *Opt. Exp.*, vol. 17, pp. 20124–20133, 2009.

[9] S. Priyadarshi, Y. Hong, I. Pierce, and K. A. Shore, "Experimental investigations of time-delay signature concealment in chaotic external cavity VCSELs subject to variable optical polarization angle of feedback," *IEEE J. Sel. Topics Quantum Electron.*, vol. 19, p. 1700707, 2013.

[10] Y. Hong, "Experimental study of time-delay signature of chaos in mutually coupled vertical-cavity surface-emitting lasers subject to polarization optical injection," *Opt. Exp.*, vol. 21, pp. 17894–17903, 2013.

[11] Z. Q. Zhong, S. S. Li, S. C. Chan, G. Q. Xia, and Z. M. Wu, "Polarization-resolved time-delay signatures of chaos induced by FBG-feedback in VCSEL," *Opt. Exp.*, vol. 23, pp. 15459–15468, 2015.

[12] S. S. Li, and S. C. Chan, "Chaotic Time-delay Signature Suppression in a Semiconductor Laser with Frequency-detuned Grating Feedback," *IEEE J. Quantum Electron.*, vol. 21, p. 1800812, 2015.

[13] T. Erdogan, "Fiber grating spectra," *J. Lightw. Technol.*, vol. 15, pp. 1277–1294, 1997.

[14] L. R. Chen, S. D. Benjamin, P. W. Smith, and J. E. Sipe, "Ultrashort pulse reflection from fiber gratings: A numerical investigation," *J. Lightw. Technol.*, vol. 15, pp. 1503–1512, 1997.

[15] S. Y. Xiang, W. Pan, L. S. Yan, B. Luo, X. H. Zou, N. Jiang, and K. H. Wen, "Quantifying chaotic unpredictability of vertical-cavity surface-emitting lasers with polarized optical feedback via permutation entropy," *IEEE J. Sel. Topics Quantum Electron.*, vol. 17, pp. 1212–1219, 2011.

[16] N. Li, W. Pan, S. Xiang, L. Yan, B. Luo, and X. Zou, "Loss of time delay signature in broadband cascade-coupled semiconductor lasers," *IEEE Photon. Technol. Lett.*, vol. 24, pp. 2187–2190, 2012.

[17] C. Cui and S. C. Chan, "Performance analysis on using period-one oscillation of optically injected semiconductor lasers for radio-over-fiber uplinks," *IEEE J. Quantum Electron.*, vol. 48, pp. 490–499, 2012.

[18] X. Z. Li, S. S. Li, J. P. Zhuang, and S. C. Chan, "Random bit generation at tunable rates using a chaotic semiconductor laser under distributed feedback," *Opt. Lett.*, accepted, 2015.

[19] S. S. Li, Q. Liu, and S. C. Chan, "Distributed feedbacks for time-delay signature suppression of chaos generated from a semiconductor laser," *IEEE Photon. J.*, vol. 4, pp. 1930–1935, 2012.